

Politecnico di Bari

Repository Istituzionale dei Prodotti della Ricerca del Politecnico di Bari

# Experimental investigation on dispersion mechanisms in rigid and flexible vegetated beds

This is a pre-print of the following article

*Original Citation:*
Experimental investigation on dispersion mechanisms in rigid and flexible vegetated beds / De Serio, F., Ben Meftah, M., Mossa, M., Termini, D.. - In: ADVANCES IN WATER RESOURCES. - ISSN 0309-1708. - STAMPA. - 120:(2018), pp. 98-113. [10.1016/j.advwatres.2017.08.005]

*Availability:*
This version is available at http://hdl.handle.net/11589/122869 since: 2021-03-09

*Published version*
DOI:10.1016/j.advwatres.2017.08.005

Publisher:

*Terms of use:*

(Article begins on next page)

17 November 2026

# Experimental investigation on dispersion mechanism in rigid and flexible vegetated beds

Francesca De Serio*[1], Mouldi Ben Meftah[1], Michele Mossa[1], Donatella Termini[2]

[1] Department of Civil, Environmental, Building Engineering and Chemistry, Polytechnic University of Bari, Italy

[2] Dipartimento di Ingegneria Civile, Ambientale, Aerospaziale, dei Materiali, University of Palermo, Italy

*corresponding author: francesca.deserio@poliba.it

## Abstract

Vegetation in channels strongly affects flow structure and turbulence, with consequences on the hydrological storage of nutrients and chemical tracers, the shelter of stream biota as well as the trapping or transport of sediments. At the same time, all these phenomena are inevitably subjected to alteration of hydrological conditions in fluvial systems due to climate change. The present study intends to provide a thorough investigation about the processes of transport and dispersion induced by flow turbulence within the vegetation structure. Specifically, velocity measurements in vegetated channels were intensively conducted and analyzed in the case of both flexible submerged and rigid emergent canopies. The experiments aimed to: i) highlight the differences in the hydrodynamic structures induced by different plant types and configurations; ii) reveal the differences in the spatially varying dispersive properties and turbulent behavior of the current, attributable to different plant density, submergence and stiffness. Further, the spatial variability of velocity and turbulence distributions was taken in due count, overlooking the commonly applied spatial averaging technique. The experimental results showed how longitudinal and transversal hydrodynamics and transport differ, depending on the vegetation arrangement and stem properties.

**keywords:** rigid vegetation, flexible vegetation, turbulent length, dispersion, advective transport.

## 1. Introduction

River vegetation has historically been acknowledged, in a hydraulic perspective, as a source of flow resistance, by increasing bottom roughness, decreasing near bed turbulent stress and reducing conveyance capacity (Nepf, 2012a,b; Camporeale et al., 2005; Gurnell, 2014). Nevertheless, the reduced velocity and transport within the vegetation shelters biota, promotes the trapping of sediments as well as the storage and retention of nutrients, chemical tracers and microbes inside the canopy, and allows flood control (Costanza et al., 1997; Kemp et al., 2000; Marois and Mitsch, 2015). Only recently vegetation has been considered as an integral part of a river system, thus its pivotal role in regulating ecological services and protecting from flood/drought risks has received

considerable attention (Nepf, 2012a,b; Pollen and Simon, 2005), also considering that the alteration of hydrological conditions is strictly sensitive to climate change.

Mean and turbulent flow, and thus both advection and dispersion, are perturbed interacting with the canopy (Ikeda and Kanazawa, 1996; Ghisalberti and Nepf, 2004; Poggi et al., 2004; Raupach and Thom, 1981; Ben Meftah et al., 2014). As a draw-back, varying water loads and change in flow characteristics affect the hydraulic behavior and resisting force of downstream plants in a community, depending on their shape, stiffness, submergence, permeability/porosity, phenologic stage (growth, maturity, decays periods). The residence time, transport and fate of contaminants, nutrients, dissolved oxygen or other scalars along with the deposition of sediment grains could be accurately envisaged depending on our ability to understand the mechanism of exchange between the free stream and the vegetated region. Such transfer mechanism is critical to the overall dispersion and seems primarily controlled by the canopy density and geometry (Oldham and Sturman, 2001; Schultz et al., 1995; Nepf et al. 2007; Ghisalberti and Nepf, 2005; Poggi et al., 2009).

To optimize the ecosystem functions and define adequate sediment management measure, a better knowledge of the impact of the changing conditions on suspended sediment mechanism should be aimed. Namely, a mutual feedback exerts between water flows, vegetation and sediments, so that the first fundamental step to recognize and manage the impacts of climate change on riverine systems is to deduce the interaction between vegetation and river hydrodynamics.

The interaction between flow and vegetation creates feedbacks to sediment deposition (Liu and Nepf, 2016), based on flow velocity and stem-generated turbulence. The deposition of fine sediment and organic material could benefit from the flow velocity reduction between the plants, whilst local soil erosion could reduce, due to the reduction of the bed shear stress (Crosato et al., 2011; Righetti and Armanini, 2002; Righetti 2008). In any case, when the main flow is diverted towards unobstructed areas, enhanced velocities laterally adjacent to the patch are produced, so that a transversal sharp transition region at the interface between the obstructed and the unobstructed domains is formed. A transverse shear occurs, generating large-scale horizontal vortices centered around the edge of the vegetated area (Lima and Izumi, 2014; White and Nepf 2007a,b; Ben Meftah et al, 2014; Ben Meftah and Mossa, 2016), which could cause localized erosion (Liu and Nepf, 2016).

The effects of vegetation on the dispersion process have been experimentally investigated for both the submerged and the emergent cases, but usually the cross section spatial averaging of non-uniform advection and diffusion results have been applied (Nepf et al., 1997; Nepf and Vivoni,

2000; Perucca et al., 2009). In this way, dispersion typically dominates the longitudinal spreading and dilution of tracers, while a uniform transversal distribution was assumed.

Experiments by Nepf et al. (1997) within an array of emergent cylindrical rods using a continuous injection technique showed that, when the plants were present, the vertical diffusivity and the diminished vertical shear reduced the shear-flow dispersion.

The production of turbulence within a stand of emergent vegetation is dominated by the stem wakes rather than by the bottom-boundary shear, as in open-channel flows (Nepf et al., 1997b). A relation between water depth and turbulence structure was highlighted by Nepf and Vivoni (2000), who pointed out that the generation of wake turbulence is strongly associated with the relative water depth. Analyses of velocity spectra and turbulent kinetic energy profiles showed that in natural river vegetation (Naden et al., 2006) and in model canopies (Ricardo et al., 2014; Zong and Nepf, 2012) stem-scale turbulence arises at stem Reynolds number $Re_d$>200, while it is absent at low $Re_d$ (Tanino and Nepf, 2008), where $Re_d$ is equal to the product of flow mean velocity and stem diameter, rated by kinematic viscosity.

For the case of rigid vegetation, Tanino and Nepf (2008) proposed a model for the mean turbulence intensity and the lateral dispersion coefficient due to the spatially heterogeneous velocity field, as a function of cylinder distribution and cylinder density. Their study proved that only turbulent eddies with mixing length scale greater than stem diameter contribute significantly to net lateral dispersion. Shucksmith et al. (2010) showed that theoretically the dominant factor influencing mixing in emergent conditions is the degree of reduction in spatial variation of velocity over the channel cross-section.

The effect of submerged vegetation on the longitudinal dispersion coefficient were investigated by Ghisalberti and Nepf (2006), who proposed a two-zone model to identify three contributing processes: large-scale shear dispersion above the canopy, inefficient exchange between the canopy and the overflow, and stem-scale dispersion within the canopy. Successively, Shucksmith et al. (2011) utilized an empirical data set of longitudinal mixing measurements to evaluate the performance of both existing and newly proposed models for mixing in submerged vegetated open channel flow. They evidenced that the rate of mixing in such systems is dependent on the relative size of the flow layers, the difference in average velocity, and the rate of transfer of mass between the layers.

Another fundamental aspect which must be considered that the physical structure of individual plants and the canopy morphology alters the velocity field across several scales (Tanino and Nepf, 2008; Nepf, 2012; Ben Meftah et al., 2014; Ben Meftah and Mossa, 2015), ranging from individual branches and blades on a single plant to a community of plants in a meadow or patch. Flow

structure at the different scales is relevant to different processes. As an example, the retention or release of organic matter, mineral sediments, seeds, and pollen from a meadow or patch depends on the flow structure at the meadow or patch scale (Mossa and De Serio, 2016; Zong and Nepf, 2011). Literature (see among others Nepf, 2012a,b; Ben Meftah and Mossa, 2013; Termini, 2016a) shows that with emergent vegetation the turbulent length scales are set by the stem diameter and spacing (Tanino and Nepf, 2008). Shucksmith et al. (2010) proved that in presence of a relatively uniform distribution of plant blockage over the width and depth, mixing is dominated by stem scale processes. In the case of dense submerged vegetation, the drag discontinuity at the top of vegetation generates a shear layer which contains canopy-scale vortices that control the exchanges of mass and momentum between the canopy and the overflow (Termini, 2015), so as the turbulent transport occurs inside the upper part of the vegetated layer.

From the brief notes above described, it is evident that the knowledge of the 'engineering' role played by vegetation in regulating eco-services and river management is crucial, even if challenging. According to Gregory et al. (1991), Lotsari et al. (2015), Sandercock and Hooke (2011), modelling should play an important role in reducing uncertainty associated with channel sensitivity and responses to threshold conditions. Strategies for quantifying solute transport in vegetated rivers consist of lumped models (Ghisalberti and Nepf, 2005), upscaled models (Marion et al., 2008) and numerical solution of the advection-dispersion equation (Rubol et al., 2016). However, the most relevant issue to both simulations and predictions is their calibration and validation. For this reason, considering that it is hard to monitor in-situ sediment/water interactions due to required timescales, laboratory experiments are needed to investigate transport patterns and dynamics for different vegetation scenarios.

Laboratory experiments in flumes provide the opportunity: i) to evaluate the impact of different hydrodynamic regimes on different plant types and configurations, in controlled conditions ii) to assess and estimate the action played by streamwise patterns of vegetation on the processes of transport and dispersion of turbulence and tracers in the three directions. The purpose of the present study is to analyze these two aspects, specifically considering the 3D spatial variability of the flow interaction with the canopy. A simple analogy could be argued to relate the solute transport of the vegetated river with its sediment transport. In any way, involving the knowledge of key parameters governing the process such as grain size or settling velocity, it goes beyond the analysis of the present research.

Experiments were carried out in two different laboratory facilities and two different types of surrogate vegetation were used. The structure of the vegetation was simplified and attention was focused on the effect of its main parameters (i.e. vegetation stiffness, density and size) on the

processes of transport and dispersion of turbulence. To this aim, plants elements having the same characteristic dimension but a different stiffness were considered and the experimental runs were conducted for different submergence and plane distribution conditions of the plants. In particular, firstly a sparse rigid and emergent canopy was studied in two different hydrodynamic configurations. Successively, a dense, flexible and submerged canopy was investigated. Considering their stiffness, density and submergence, they could be intended as representative of different grow stages of a vegetation system in a river.

The paper is structured in the following way. In the next section a theoretical background is provided to point out the principal variables involved in the process of turbulence transport, which resembles solute transport. In section 3 the experimental work is illustrated, while results from the two canopies are analyzed in Section 4 and finally discussed in Section 5.

## 2. Theoretical approach

### *2.1 Main variables involved*

Canopy consists of a distribution of plants elements. In the present paper both rigid cylinders of uniform diameter $d$ and submerged canopy of blade width $d$ have been considered. Thus, according to Ghisalberti and Nepf (2009) it is reasonable to define $d$ as the characteristic element scale within the canopy. Other key parameters characterizing the canopy are the solid volume fraction $\phi$, i.e., the volume within the canopy occupied by solid elements, which is the complement of the canopy porosity $\eta=1-\phi$ and the frontal area per unit length of the canopy $a=nd$, where $n$ is the number of elements per unit planar area. In the case of a periodic square array of cylinders, named $s$ the axis-to-axis distance of the cylinders, the value of $a$ is equal to $1/s^2$. Within the array the flow is spatially heterogeneous at the scale of the individual elements and often unsteady in time. Generally, in the case of obstructed flows the double-averaging method is used to remove the temporal and element-scale spatial heterogeneity of the current (Raupach and Shaw, 1982; Finnigan, 1985). In other words, the instantaneous equations of the vegetated current are first averaged over a time longer than the time scale of turbulence or instabilities in the flow and then averaged over an infinitesimally thin area that spans many cylinders, including only the area occupied by the fluid. In the present study, only the time-averaging procedure (indicated by the overbar sign) is used, to not miss information on the typical spatial variations in the longitudinal and transversal sections. For the sake of simplicity, the ambient current is considered uniform.

*2.2 Solute transport and contribution from turbulence*

Hereafter we consider a rectangular canopy located in a fluid of depth *H*. The canopy length is parallel to the mean flow directions with *u*, *v* and *w* the streamwise, transverse and vertical velocity components, respectively. The *x*-axis is parallel to the mean flow and sits along the centerline of the channel and array. The *y*-axis is at the leading edge of the canopy and is perpendicular to the mean flow direction. The profile of the current velocity upstream of the canopy is assumed uniform over the water depth.

The transport of a tracer *c* (species concentration) is described by the following expression:

$$\frac{\partial c}{\partial t} + \mathbf{v} \cdot \nabla c = -\nabla \cdot \left( -D_0 \nabla c \right) \tag{1}$$

where $t$ is time, $c(\mathbf{x},t)$ is the solute concentration, $\mathbf{v}(\mathbf{x}, t)=(u,v,w)=(v_1,v_2,v_3)$ is the fluid velocity, $D_0$ is the molecular diffusion coefficient and $\mathbf{x}=(x,y,z)=(x_1,x_2,x_3)$. Neglecting the molecular diffusion, that is small in a turbulent flow, and time averaging eq. (1) over a time interval much longer than the time scales of turbulent fluctuations, we have the time-averaged concentration equation

$$\frac{\partial \bar{c}}{\partial t} + \frac{\partial \overline{u_j}\,\overline{c}}{\partial x_j} = -\frac{\partial \overline{u_j' c'}}{\partial x_j} \tag{2}$$

where the overbar denotes the temporal average and the prime symbol denotes the temporal fluctuations, so that

$$\begin{aligned} c(\mathbf{x},t) &= \bar{c}(\mathbf{x}) + c'(\mathbf{x},t) \\ u(\mathbf{x},t) &= \bar{u}(\mathbf{x}) + u'(\mathbf{x},t) \\ v(\mathbf{x},t) &= \bar{v}(\mathbf{x}) + v'(\mathbf{x},t) \\ w(\mathbf{x},t) &= \bar{w}(\mathbf{x}) + w'(\mathbf{x},t) \end{aligned} \tag{3}$$

Equation (2) shows that the concentration mass flux is due to the convection by the time-averaged flow (also named mean flow), $\overline{u}\,\overline{c}$, $\overline{v}\,\overline{c}$ and $\overline{w}\,\overline{c}$, and transport by turbulent velocity fluctuations, $\overline{u'c'}$, $\overline{v'c'}$ and $\overline{w'c'}$.

Equation (2) can be rewritten as follows

$$\frac{\partial \bar{c}}{\partial t} + \frac{\partial \overline{u_j}\,\bar{c}}{\partial x_j} = K_{jj}\frac{\partial^2 \bar{c}}{\partial x_j^2} \tag{4}$$

In fact, following Ting and Kirby (1995, 1996), in direct analogy to turbulent momentum transport, also turbulent mass concentration transport is assumed to be related to the gradient of the transported quantity. In this way, $K_{jj}$ are the coefficients for net dispersion, which parameterize $\overline{u_j'c'}$, i.e. the turbulent diffusion.

Furthermore, the terms $\overline{u_j'c'}$, like the molecular diffusion, are expected to be Fickian if the spatial scale of the contributing mechanisms is smaller than the scale over which the mean concentration gradient varies. The mechanisms associated with the terms $\overline{u_j'c'}$ have characteristic scales of the stem diameter *d* and axis-to-axis distance *s*.

Differently from Tanino and Nepf (2008), who averaged eq. (1) both in time and in space, in our present case the flow is three-dimensional and, therefore, the equations are only time-averaged. This means that the present study focuses on the turbulent diffusion, whereas the mechanical dispersion is the consequence of the time-averaged spatial fluctuations (Tanino and Nepf, 2008).

In the analysis of the flow-dispersion interaction, the turbulent kinetic energy (TKE) is important in determining the turbulent dispersion coefficient and thus the mass transport. The turbulent dispersion coefficient may be written as the product of a length scale and a velocity scale. A physical meaningful velocity scale is $\sqrt{k}$, where *k* is the turbulent kinetic energy, i.e.

$$\begin{aligned} k &= \overline{k'} = \frac{1}{2}\overline{u_i'u_i'} \\ k' &= \frac{1}{2}u_i'u_i' \end{aligned} \tag{5}$$

Therefore, the determination of the time and spatial variations of turbulent kinetic energy is of great importance in the evaluation of the dispersion process. For high Reynolds number the equation of the turbulent kinetic energy is

$$\underbrace{\frac{\partial k}{\partial t}}_{\text{Local derivative}} + \underbrace{\frac{\partial \overline{u_j} k}{\partial x_j}}_{\text{Advection}} = -\frac{\partial}{\partial x_j}\left( \underbrace{\frac{1}{\rho}\overline{u_j' p'}}_{\text{Pressure diffusion}} + \underbrace{\overline{u_j' k'}}_{\text{Turbulent transport}} \right) - \underbrace{\frac{1}{2}\overline{u_i' u_j'}\left( \frac{\partial \overline{u_i}}{\partial x_j} + \frac{\partial \overline{u_j}}{\partial x_i} \right)}_{\text{Production}} - \underbrace{\frac{1}{2}\nu \overline{\left( \frac{\partial u_i'}{\partial x_j} + \frac{\partial u_j'}{\partial x_i} \right)^2}}_{\text{Dissipation}} \quad (6)$$

Following Nepf (1999), we assume that the production term is of order of the dissipation term. This assumption is justified by Nepf (1999)'s experimental results. Considering the production of TKE as sum of wake production and bed shear production, Nepf (1999) noted that the bed shear production was negligible over almost the flow depth, except than very close to the bed. Consequently, TKE dissipation and wake production balanced over almost the flow depth, except than close to the bottom.

Furthermore, to obtain the diffusive transport terms, in turbulence modeling, turbulent diffusion is often assumed proportional to the gradient of $k$ (Rodi, 1984), i.e.

$$-\left( \frac{1}{\rho}\overline{u_j' p'} + \overline{u_j' k'} \right) = D_k \frac{\partial k}{\partial x_j} \quad (7)$$

with the turbulent diffusion coefficient $D_k$

$$D_k = \frac{\nu_t}{\sigma_k} \quad (8)$$

where $\nu_t$ is the eddy viscosity and $\sigma_k$ is an empirical diffusion constant. Therefore, being energy dissipation and production of the same order of magnitude, the transport equation for $k$ becomes

$$\frac{\partial k}{\partial t} + \frac{\partial \overline{u_j} k}{\partial x_j} = D_k \frac{\partial k}{\partial x_j} \quad (9)$$

where, following the eddy-diffusivity concept (Ting and Kirby, 1995; Nepf, 1999), the turbulent diffusion coefficient is assumed as

$$D_k = l\sqrt{k} \quad (10)$$

with $l$ the integral length scale associated with turbulent eddies. Equation (9) is formally analogous to eq. (4) and, therefore, assuming that the Prandtl number is O(1), the analysis of the terms of

eq. (9) can be used for eq. (4).

Consequently, it seems interesting to investigate the relations between $\bar{u}$, $\bar{v}$, $\bar{w}$ and *k*. In fact, the analogy between eq. (4) and eq. (9) suggests that the cross-correlation between the time-averaged turbulent kinetic energy and the $\bar{u}$, $\bar{v}$ and $\bar{w}$ velocity components is related to the time-averaged solute concentration $\bar{c}$ transport by the mean flow, $\overline{uc}$, $\overline{vc}$ and $\overline{wc}$.

This approach was also used by Ting and Kirby (1994), who stated that the suspended sediment concentration shows that the mass flux along the flow direction is due to convection by mean flow and transport by turbulent velocity fluctuations, while the tendency of sediment to settle out is counteracted by the action of turbulent fluctuations. In their study, they proved that if it is assumed that turbulent velocity fluctuations are responsible for keeping sediment in suspension, and the mean flow transports the sediment, then suspended sediment transport resembles turbulence transport.

In the present study, sediments were not directly investigated and consequently some key parameters, like grain size or settling velocity, were not available to examine thoroughly the analogy between the transport of TKE and the sediment transport. In any way, the analogy between the transport of TKE and the transport of a scalar concentration by means of the mean flow is reliable and is taken into consideration, referring to both eq. (4) and eq. (9).

The integral length scale *l*, present in eq. (10), can be evaluated by the power spectrum or by multiplying the integral time scale $T_u$ by the local time-averaged velocity $\overline{u_i(\mathbf{x})}$, where $T_u$ is estimated by the autocorrelation function of the turbulent velocity fluctuations, i.e.

$$l_i = \overline{u_i(\mathbf{x})} \cdot T_u = \overline{u_i(\mathbf{x})} \cdot \int_0^{\tau_0} \frac{u_i'(\mathbf{x},t) \cdot u_i'(\mathbf{x},t+\tau)}{\overline{u_i'^2(\mathbf{x})}} d\tau \tag{11}$$

with $\tau$ the time lag with respect to *t* and $\tau_0$ the value of $\tau$ at the first zero-crossing.

The integral length scale of turbulence *l* depends strongly on the presence of cylinders. In unobstructed flow, *l* increases with the scale of the diffusion patch until the largest length scale is reached, that is the length scale defined by the flow domain (Okubo, 1971). Emergent canopies impose structure on both the mean and turbulent flow over the entire water column. In flows with emergent vegetation, the canopy dissipates eddies with scales greater than the stem scale of *s* and *d*, while contributing additional turbulent energy at these stem scales. Thus, the dominant turbulent length scale within a canopy is shifted downward from analogous condition without vegetation. Particularly, in a channel with a regular array of cylinders, the integral length scale of the turbulence

is set by the smaller of the stem diameter, $d$, or the distance between the stems $s$, regardless of the water depth (Taylor, 1935; Tanino and Nepf, 2008). In other words, for $d \leq s$, turbulence is generated within stem wakes (if the $Re_d$ is larger than 120) so that $l=d$; on the contrary, for $d>s$, turbulence is generated within the pore channels so that $l=s$.

These two depicted regimes in presence of cylinders are not exhaustive, since for low solid volume fractions ($ad$ less than 0.01) the integral length scale of the turbulence should have an intermediate value between those previously mentioned, i.e. $l=O(\min(d,s)\div H)$. For further details, see for example Nepf et al. (1997) and Lopez and Garcia (1998).

Analogously to eq. (10), Tanino and Nepf (2008) assumed that the net dispersion coefficients could be assumed equal to

$$K_{jj} = \alpha \sqrt{k} l_j \tag{12}$$

where the scale factor $\alpha$ could generally differ for horizontal and vertical diffusion.

Following Nepf (1999), it is reasonable to assume the horizontal dispersion coefficient value in the range [0÷1].

## 3. METHODS AND MATERIALS

Literature (Nepf, 2012a,b) shows that aquatic plants exhibit a wide range of geometry and distribution ranging from relatively sparse with $a$=1 to 7m$^{-1}$ and $\phi$=0.1% to densest canopies with $a$ up to 20m$^{-1}$ and $\phi$=1%. Specifically, seagrasses are generally submerged and tend to have solid volume fraction variable from 1% and 10%; emergent plants tend to have rounded stems for higher stiffness and submerged grass tend to have a blade geometry in which the width (ranging between 0.3 and 1cm) is larger than the thickness.

Based on the above information, two flow velocity datasets have been used in this work: the first one (herein indicated as BA-R data set) was collected with the bed covered by rigid emerged vegetated stems; the second one (herein indicated as PA-F data set) was collected with flexible and submerged vegetation on the bed. The vegetation elements were characterized by the same characteristic dimension $d$. The manifest diversity of the two vegetated systems is justified by the aim to identify the key parameters which drive their different behaviors and find possible analogies in the hydrodynamic and dispersion processes.

*3.1 Setup and instrumentation for the rigid vegetated flume (BA-R data set)*

Experimental runs were carried out in a smooth horizontal rectangular channel in the Department of Civil, Environmental, Building Engineering and Chemistry of the Technical University of Bari (Italy). The channel was 25.0 m long, 0.40 m wide and 0.50 m deep, with lateral walls and bottom surface in Plexiglas, as shown in Figure 1. A stable recirculating flow was guaranteed in the channel. For details please refer to Ben Meftah and Mossa (2013) and Ben Meftah et al. (2015).

The vegetation array was constructed of vertical, rigid, circular steel cylinders, with threaded lateral surfaces and thus considered as rough cylinders. The cylinder diameter was $d$ =0.003m. The cylinder extremities were inserted into a plywood plaque 3.0m long, 0.02m thick and a width equal to those of the channels, which in turn was fixed along the channel bottoms, forming the experimental area. The plywood plaque was extended 3m both upstream and downstream of the array of cylinders (experimental area) and was tapered to the channel bottom to minimize flow disturbance (Figure 1). Cylinders were arranged regularly and spaced longitudinally and transversally with the same axis-to-axis distance $s$=0.05m, so that the cylinder density, $n$, was 4 cylinders/dm$^2$, while the vegetation density per meter was $a = 1.2$ m$^{-1}$ and the solid volume fraction was $\phi$= 0.28%. Therefore, following Nepf (2012a), reasonably this vegetation can be considered sparse.

A Cartesian coordinate system ($x$, $y$, $z$) was adopted, in the centre of the array, with $x$-, $y$- and $z$-coordinates denoting the longitudinal, transversal and vertical directions, respectively. Because water was forced to move around the cylinders, the flow within the canopy was turbulent and highly heterogeneous at the scale of the individual stem. Therefore, the instantaneous three-dimensional flow velocity components, through different longitudinal, cross and horizontal planes, were accurately measured (1cmx1cm grid resolution) using a down looking three-dimensional Acoustic Doppler Velocimeter (ADV)/Vectrino system by Nortek. The ADV was used with a velocity range equal to ±0.30m/s, a velocity accuracy of ±1%, a sampling rate of 100Hz and a sampling volume of vertical extend of 9mm. The acquired data were filtered based on the Tukey's method (Ben Meftah, et al. 2015) and bad samples (signal-to-noise ratio SNR<15db and correlation coefficient<70%) were removed. Measurements were carried out placing the ADV between two successive rigid stems.

Two different runs were analysed, with different flow depth and mean channel velocity, named BA-R1 and BA-R2. The initial experimental conditions and parameters of the runs are shown in Table 1. Herein, $B$ is the channel width and $Fr=U_a/(gH)^{0.5}$ is the inlet flow Froude number, with $U_a$(=$Q$/$BH$) the mean channel velocity, $g$ the gravity acceleration and $Q$ the flow rate. The element Reynolds number $Re_d$ was calculated based on $d$ and on the time-averaged velocity, also averaged

in the transversal plane.

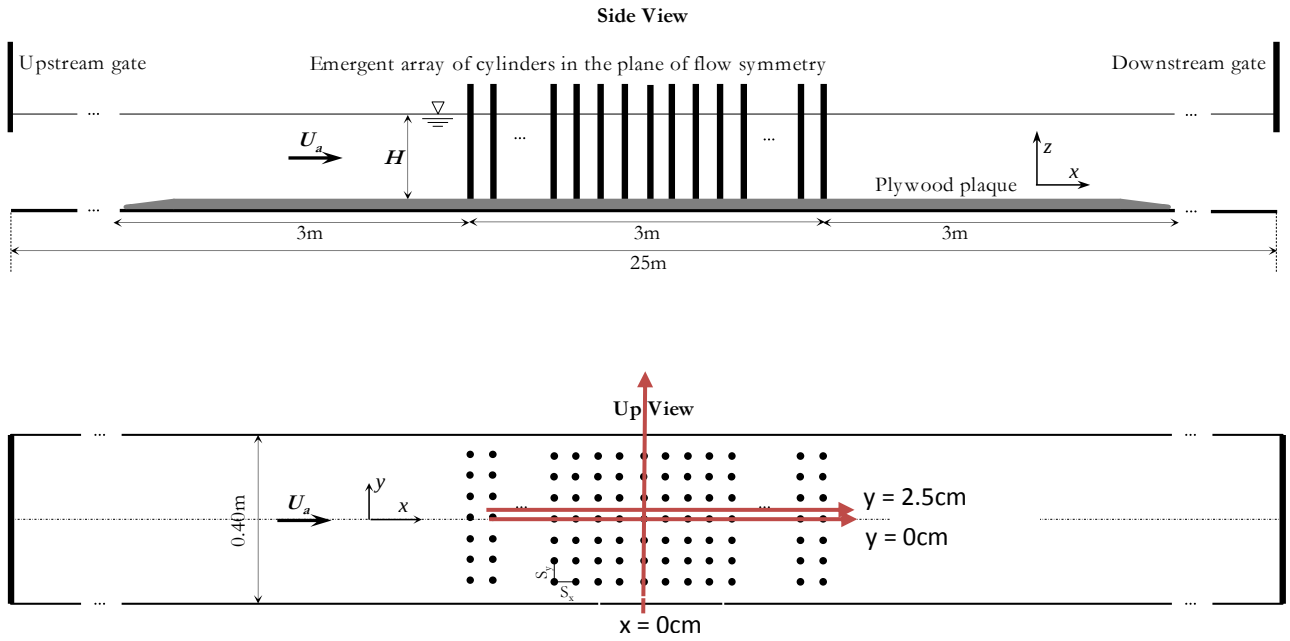



**Figure 1**. Definition sketch of the channel with the array of cylinders. BA-R data set.

*3.2 Setup and instrumentation for the flexible vegetated flume (PA-F data set)*

The data used for such a comparison were collected in a straight laboratory channel constructed at the Hydraulic Laboratory of DICAM Department of University of Palermo (Italy). Details of the experimental apparatus and measurement conditions can be found in previous works (Termini and Sammartano, 2012; Termini, 2013; 2016). Thus, only information important for the following analysis is reported in this section. The rectangular flume is 11.2 m long and 0.4 m wide (see Figure 2). The longitudinal bed slope is equal to 0.4% and the channel reach (1.60 m long) downstream of the initial section X0 (see Figure 2) was covered by real herbaceous (flexible) vegetation (*Festuca arundinacea*). The vegetation stems have a blade geometry with width $d$ =0.003m. Experimental run was conducted with water discharge $Q$ = 35l/s. The vegetation height $H_v$ (that is the height before producing submergence of vegetation) was about equal to 7.8 cm and the bent vegetation height $k_v$ was about equal to 2.6 cm. The stems concentration was equal to 190 stems/dm$^2$ at which corresponds a value of the fractional plant area equal to $\phi$=13.5% and $a$=57m$^{-1}$, so that this canopy can be considered dense (Nepf, 2012a,b). The element Reynolds number was $Re_d$= 2466.

During this run the instantaneous longitudinal $u(t)$, transversal $v(t)$ and vertical $w(t)$ velocity components were measured by using the DOP 2000 Profiler by Signal Processing s.a. Three probes of emitting frequency of 8MHz were used. The DOP2000 allowed the measurement of the

instantaneous flow velocity profile along the direction of each probe. Details of the measurement conditions can be found in Termini (2013; 2016a,b).

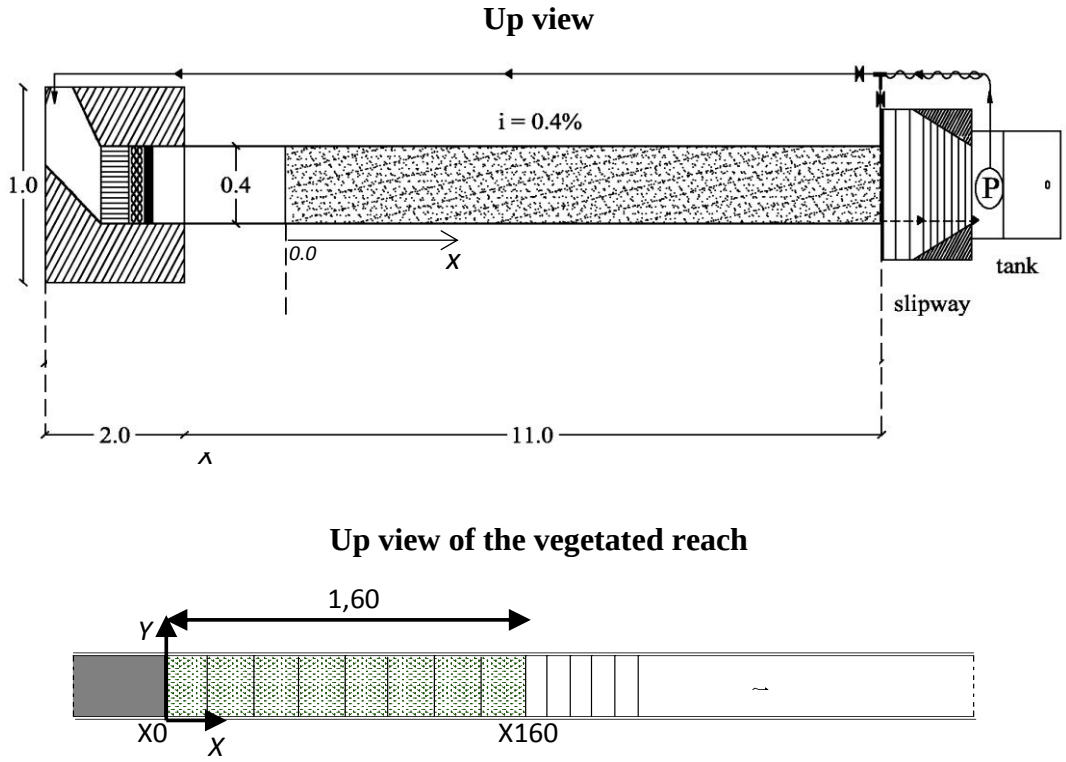



**Figure 2.** Definition sketch of the vegetated channel. PA-F data set. All measurements are in meters.

| **Run** | $H$ (m) | $Q_a$ ($m^3/s$) | $U_a$ (m/s) | $Re_d$ | $F_a$ | $d$ (m) | $a$ ($m^{-1}$) |
|---|---|---|---|---|---|---|---|
| BA-R1 | 0.37 | 0.024 | 0.16 | 480 | 0.081 | 0.003 | 1.2 |
| BA-R2 | 0.30 | 0.023 | 0.19 | 629 | 0.111 | 0.003 | 1.2 |
| PA-F | 0.11 | 0.035 | 0.82 | 2466 | 0.804 | 0.003 | 57 |

**Table 1.** Initial conditions and parameters of the experiments.

## 4. RESULTS

The two experiments are described separately, examining the distributions of the time averaged horizontal velocity, turbulent kinetic energy, integral length scales and diffusivity coefficients. Further the advective transport of the turbulent kinetic energy due to the mean flow is also investigated. For the sake of simplicity, afterwards the time-averaged longitudinal, transversal and vertical velocity components, $\overline{u}$, $\overline{v}$ and $\overline{w}$, will be also referred as *U*, *V* and *W*, respectively.

*4.1 Results of BA-R data set*

For this data set, in BA-R1 run values assessed along the longitudinal planes *y*=2.5cm (i.e. *y/d*=8.3) and *y*=0 (i.e. *y/d*=0) are available; in BA-R2 run values assessed along the longitudinal planes *y*=2.5cm (i.e. *y/d*=8.3) are available.

As an example, Figure 3a shows for BA-R1 case the typical cylinder effects on the flow velocity distribution in the horizontal plane, computed as $Ut = \sqrt{U^2 + V^2}$, at the intermediate depth *z/H*=0.45 (for further details, please refer to Ben Meftah and Mossa, 2013; Ben Meftah et al., 2014; Ben Meftah et al., 2015). Because of the ADV technical limitations, measurements were not assessed in the uppermost layer, with a thickness of 7cm. A typical trend is observed in the mapped flow, with the expected behavior of the velocity, showing maxima values in the intermediate position between two consecutive cylinders where the flow converges. As well, the flow diverges from each cylinder, inducing the typical wake. Figure 3b displays for BA-R1 run the vertical profiles of the time-averaged longitudinal *U* velocity (normalized by *Ua*) and plotted for different *x/d* positions along the longitudinal section at y/d=8.3. The *x* positions are all located 0.03m downstream of a cylinder, thus in the region of higher velocity. As previously written, the 3D flow is sensitive to the investigated position relative to the stems. In fact, observing Figure 3b, we note that the vertical trends of *U* normalized by *Ua* are different depending on the relative measuring position *x/d* with respect to the stems. In any way, to allow a straightforward data comparison, the longitudinal average of the vertical profiles was considered too and plotted on the same graph (red line). This longitudinally-averaged profile of *U/Ua* was obtained by averaging the data of the different *x/d* positions at the same *z/H*. As expected, reduced values of the *U/Ua* profile are noted in comparison with those of the bare channel (i.e. unobstructed flow), superimposed in Figures 3b (green line). Analogous profiles are shown for BA-R2 run and *y/d*=8.3 in Figure 3c, where a flattened longitudinally-averaged profile of *U/Ua* is also displayed for the vegetated case with respect to the unobstructed channel case.

Figures 4a and 4b plot the vertical profiles of the time-averaged turbulent kinetic energy, normalized by $U_a^2$ for *y/d*=8.3 of BA-R1 and BA-R2 case, respectively. Also in this graphs the green and red lines are shown, still referring to the unobstructed flow and to the longitudinally-averaged profile of the vegetated flow, each. In presence of vegetation, increased turbulent kinetic energy values *k* at all depths and at all *x/d* positions are evident, if compared to the not vegetated flow, thus proving the increased turbulent effect induced by the rigid stems on the flow. Moreover, in the unobstructed flow greater values of *k* are noted near the bed as expected, especially for the BA-R1 run (Figure 4a), with a decreasing trend towards the surface. For the vegetated flow, near the surface, few higher values of normalized *k* of BA-R1 run are noted, attributable to unavoidable

local instabilities.

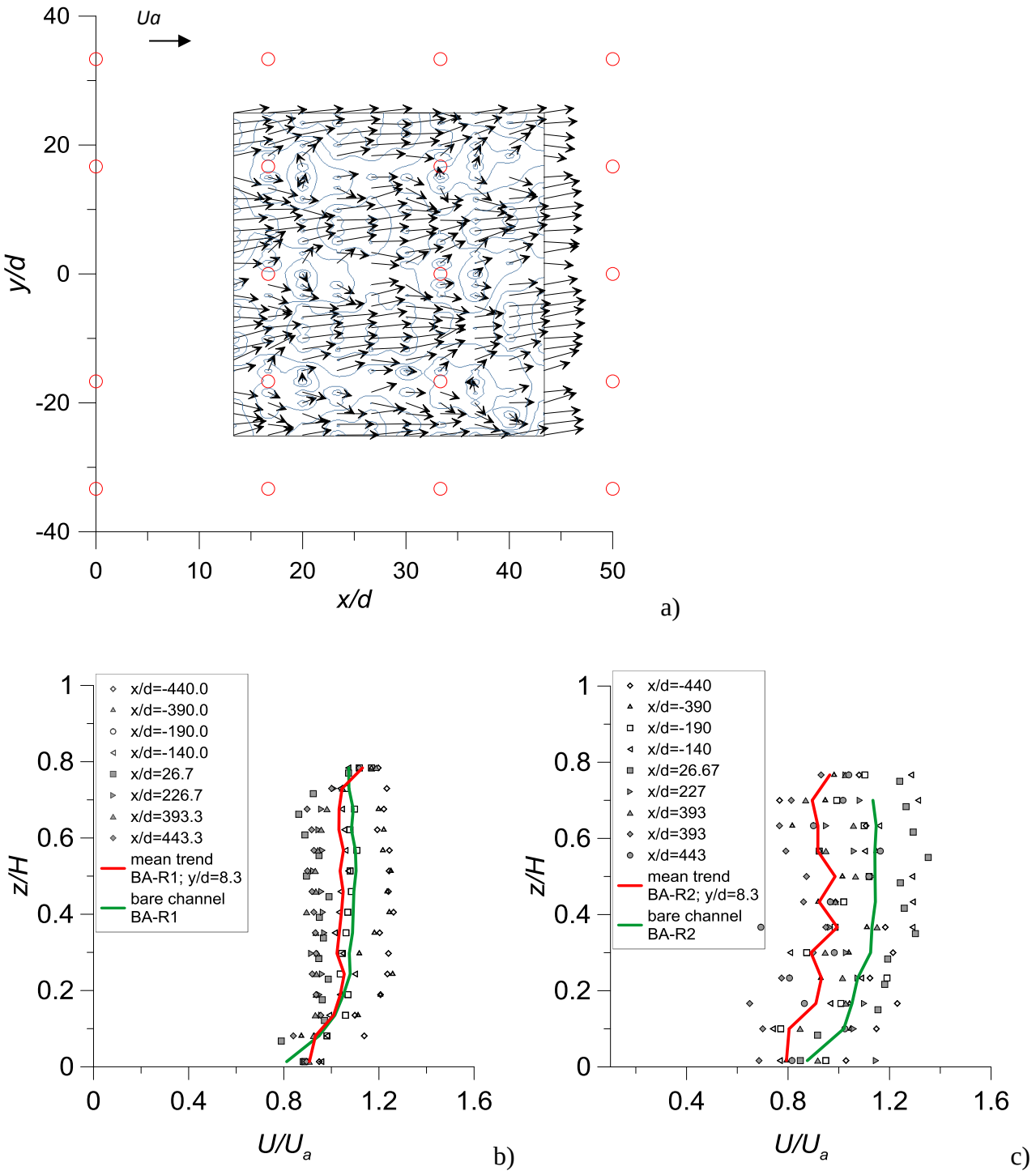



**Figure 3.** a) Horizontal map of the flow velocity distribution in the plane (*xy*) at *z/H*=0.45 for BA-R1 data set; b) vertical profiles of *U/Ua* velocity component in the longitudinal section *y/d*=8.3 at all the investigated *x/d* positions for BA-R1 data set and c) BA-R2 data set. The green line shows the trend for the unobstructed case, while the red line shows the longitudinally-averaged profile.

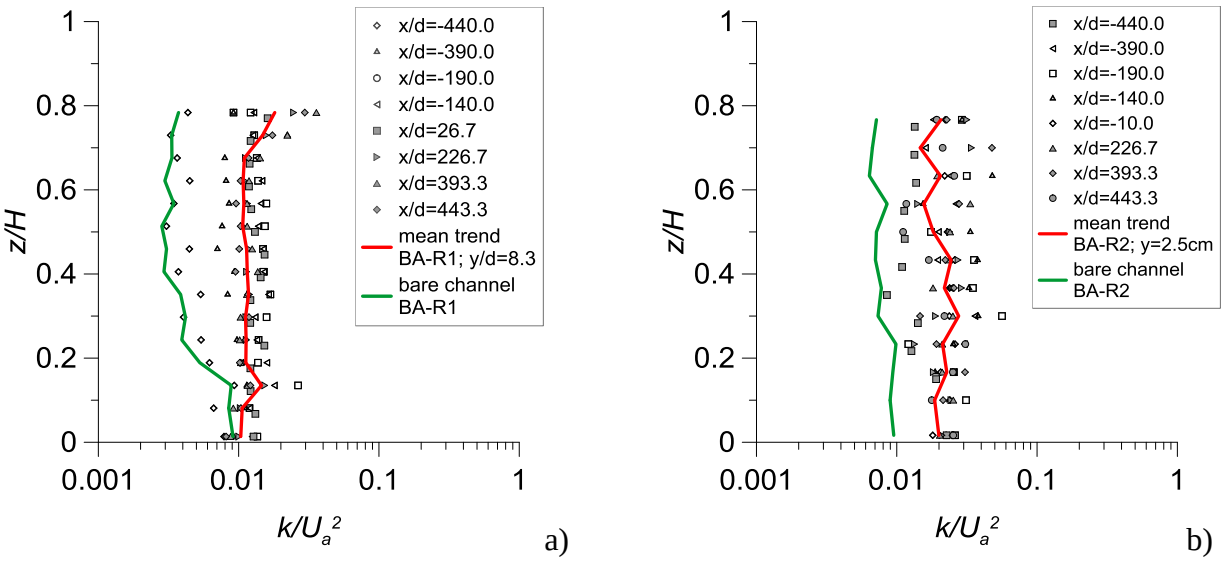



**Figure 4.** Vertical profiles of the normalized turbulent kinetic energy in the longitudinal plane *y/d*=8.3 a) BA-R1 data set; b) BA-R2 data set

For the successive key parameters, the analysis is structured in the subsequent way. Firstly, the BA-R1 run is described referring to all values measured at each *x/d* position along the longitudinal section *y/d*=8.3. In this way, the local variability of the parameters is evident. Successively, to have a global view, the longitudinally averaged vertical profiles (mean trends) of the vegetated case *y/d*=0 of BA-R1 run and y/d=8.3 of BA-R2 run were also added in the graphs. The vertical trends of both BA-R1 and BA-R2 unobstructed cases were also overlaid. In this way, the grouped trends allow a thorough understanding of the dispersion process.

The analysis of Figure 5 shows the integral turbulent lengths, normalized by *d*, along the three directions, i.e. *lx*, *ly* and *lz*, calculated by means of eq. (11), referring to all points investigated in BA-R1 run, in the longitudinal plane *y/d*=8.3. As previously written, in the case of the unobstructed channel, the integral length scale of turbulence *l* is of order of the channel flow depth *H*. Instead, the presence of the array, its density and arrangement of the plants, modify the structure of the turbulent flow (Righetti, 2008). In fact, it is worth noting that, for the bare channel flow values of *lx* are of the same order of magnitude of the channel height, i.e. $O(10^{-1})$, consistently with Okubo (1971) and Nepf (1999). The presence of the vegetation induces a reduction of *lx*, which is characterized by a lower order of magnitude with respect to the unobstructed case, i.e. $O(10^{-2})$ and comparable with the canopy pore *s*. On the contrary, in the transversal direction, the length *ly* increases when the vegetation is present, with respect to the not vegetated case, even if the order of magnitude of *ly* is $O(10^{-4})$ for both unobstructed and obstructed cases. The turbulent length *lz* in the vertical direction is reduced in the obstructed flow in comparison with the unobstructed case, keeping the same order of magnitude $O(10^{-4})$. The behavior observed in Figure 5 highlights that the turbulent eddies are

affected by the symmetrical and equally spaced rigid stems, thus becoming flattened in the longitudinal and vertical directions while they stretch in the transversal one.

For *lx*, *ly* and *lz*, Figure 6 collects the vertical profiles of the unobstructed flow of BA-R1 and BA-R2, as well as the longitudinally averaged vertical profiles (mean trends) of BA-R1 for $y/d$=0 and $y/d$=8.3 and of BA-R2 for $y/d$=8.3. Three different logarithmic abscissa axis are inserted, to identify if the turbulent length scale is scaled by *d*, *s* or *H* (considering that *H* is different for BA-R1 and BA-R2 runs, the reference value $H$=0.3m was used).

Namely, the analysis of *lx* (Figure 6) is interesting and marks the novelty of the present research. In fact, as previously written, in the present case of sparse vegetation with $ad$<O(0.01), it was expected that the integral length scale of turbulence was of O(*d*), consistently with Nepf et al. (1997) and Lopez and Garcia (1998).

Figure 6a confirms that when vegetation is absent (bare channel BA-R1 and bare channel BA-R2) *lx* has the order of magnitude of *H*. In addition, it reveals that when $y/d$=8.3, *lx* has the order of magnitude of *s*; while when $y/d$=0, *lx* has the order of magnitude of *d*. Therefore, for this sparse rigid vegetation a heterogeneous and locally variable behavior of *lx* is proved. It depends not only on the density of the canopy but also on the position relatively to the stems. For the longitudinal plane $y/d$=8.3 (in both BA-R1 and BA-R2 runs) where in-line stems are absent (Figure 1), turbulent eddies tend to occupy all the available stem-to-stem distance and *lx* is scaled by *s*, which on the contrary should occur when $d>s$, according to previous research. In contrast, for the longitudinal plane $y/d$=0 (BA-R1 run) where in-line stems are present (Figure 1), turbulent eddies are in the stem wake and blocked by the same stems, so that the canopy behaves as expected.

In Figure 6b the mean trends of *ly* are assembled for all the investigated cases. It is evident that *ly* is increased of about one order of magnitude by the presence of the stems. The mean trends of *lz* are shown in Figure 6c, where the presence of the stems induces a reduction of about one order of magnitude, specifically in the BA-R1 case for $y/d$=0.

For BA-R1 run and $y/d$=8.3 the vertical profiles of the dispersion coefficients *Kxx*, *Kyy* and *Kzz*, computed with eq. (12) using $\alpha$=0.9, are plotted in Figure 7, normalized by $U_a d$. The coefficients *Kxx* and *Kyy* display trends resembling those of the corresponding turbulent lengths. In fact, in the longitudinal direction, the dispersion coefficients are reduced by the presence of vegetation, while they increase in the transversal direction. Referring to *Kzz*, the two vertical profiles, of the unobstructed flow and of the vegetated flow longitudinally averaged, show analogous trends.

The global view of the dispersion coefficients is shown in Figure 8, where all the mean trends are assembled. The above described tendencies are confirmed. Specifically, the reduction of *Kxx* for BA-R1 run and $y/d$=0 is noteworthy. As well, the vertical dispersion is negligible if compared to the

longitudinal and transversal one.

Figure 9 displays for BA-R1 run and $y/d$=8.3 the advective transport of $k$ by the time-averaged flow in the longitudinal, transversal and vertical direction, normalized by $U_a^3$. The spatially averaged transport in the transversal and vertical directions is around zero, for both cases of obstructed and unobstructed flow, except for a few points approaching the surface due to local effects.

In the longitudinal direction, instead, it is increased by the presence of the rigid stems, with respect to the not vegetated case. In fact, higher $k$ values of the vegetated case play an essential role in the product $Uk$. The global trend of Figure 10 furtherly confirms this observation.

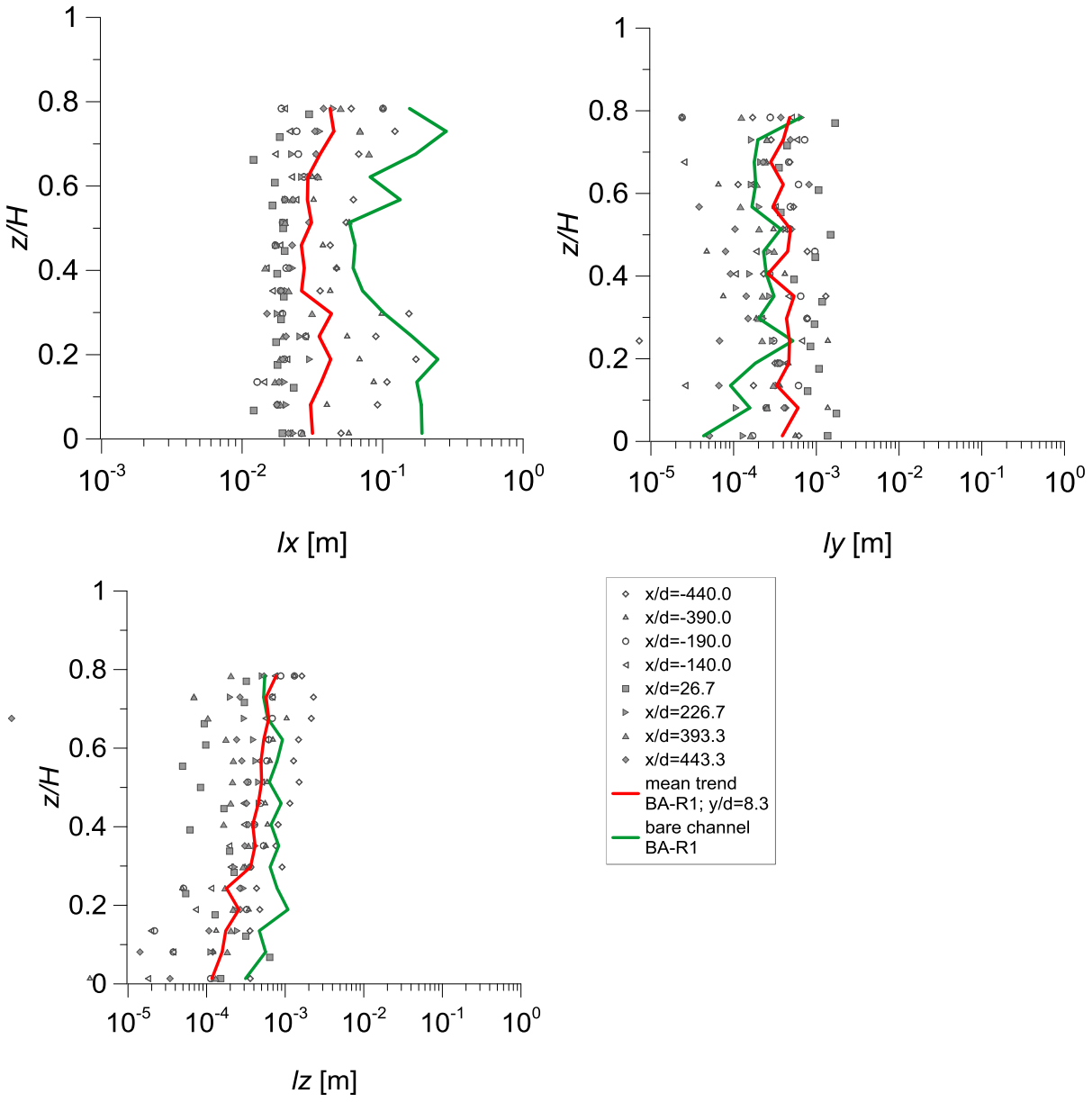



**Figure 5.** Vertical profiles of integral length scales *lx*, *ly* and *lz*, in the longitudinal $y/d$=8.3. BA-R1 data set.

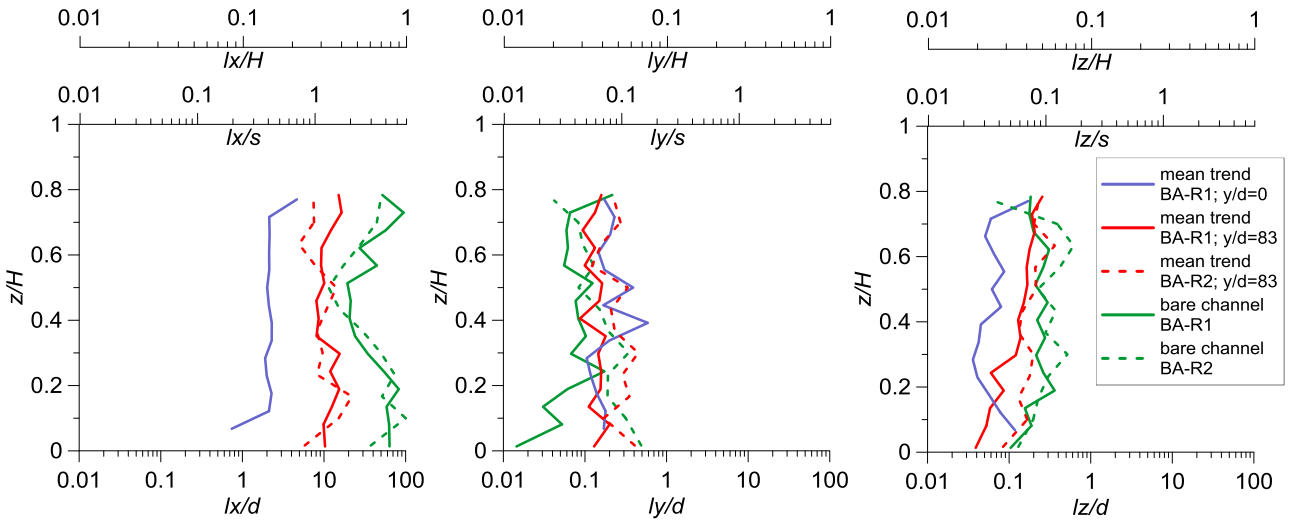
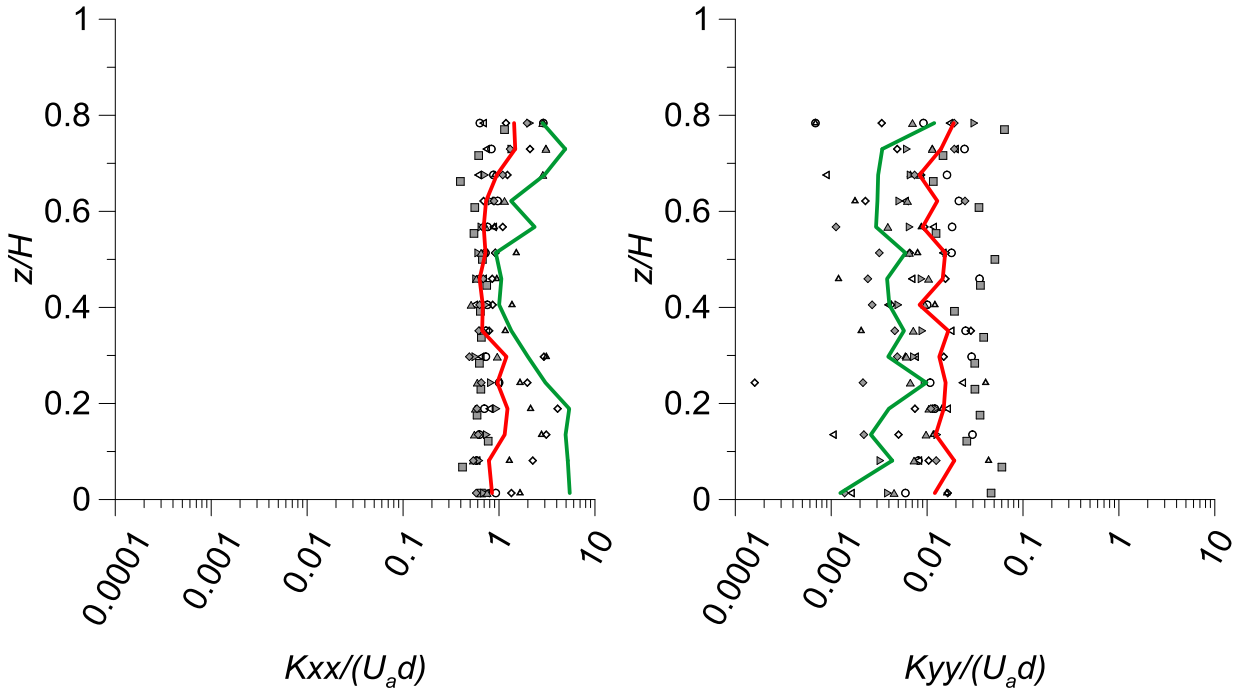



**Figure 6.** Mean vertical profiles of integral length scales *lx*, *ly* and *lz*, for all the assessed data.



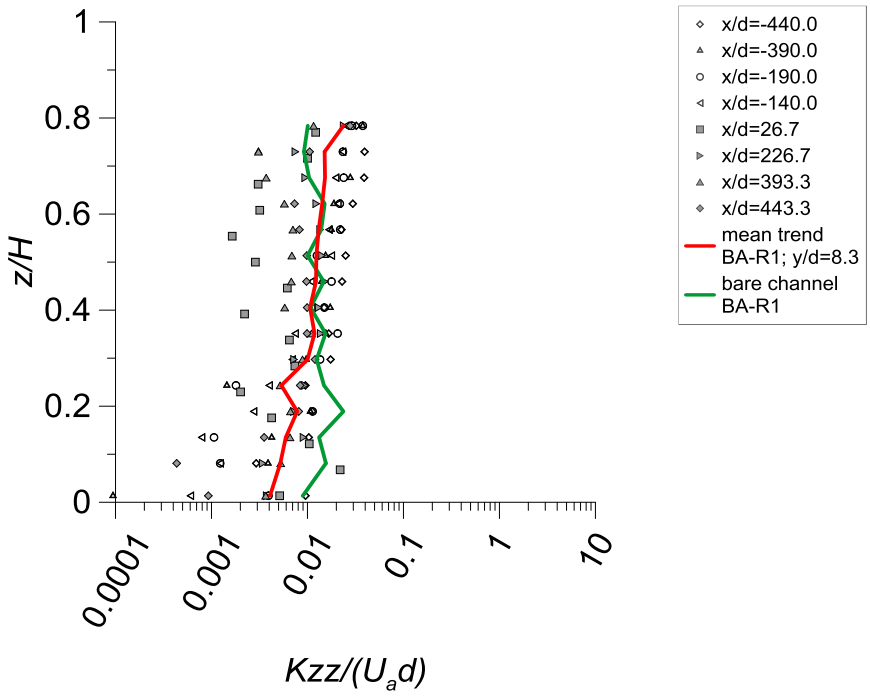



**Figure 7.** Vertical profiles of dispersion coefficients *Kxx*, *Kyy* and *Kzz*, in the longitudinal plane *y/d*=8.3. BA-R1 data set.

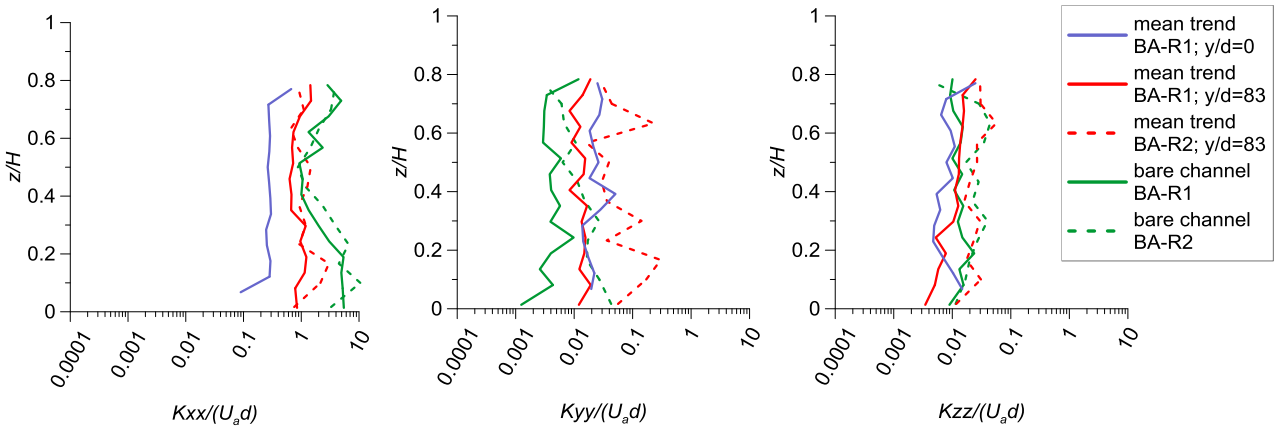



**Figure 8**. Mean trend of vertical profiles of dispersion coefficients for all the assessed data.

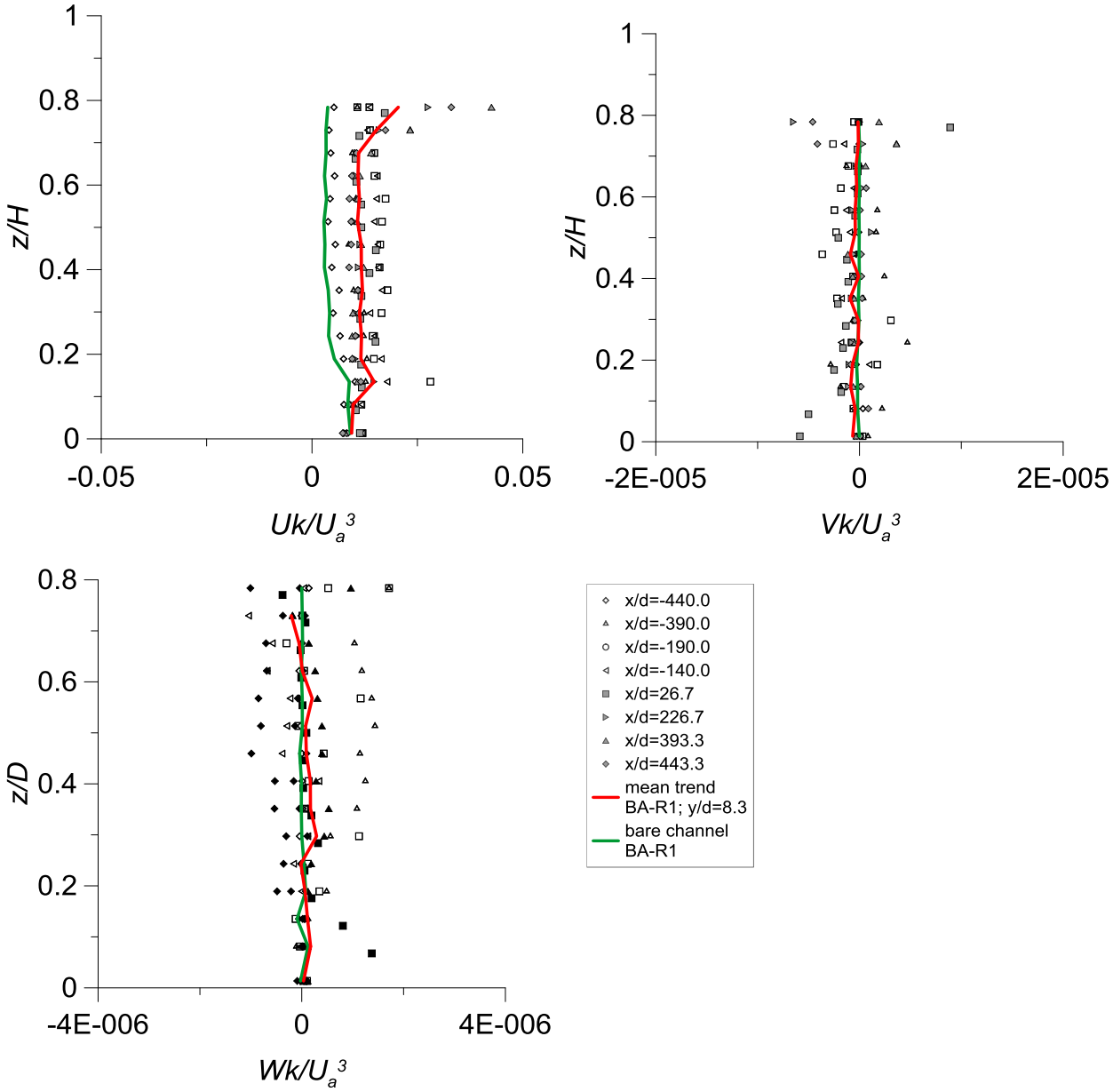



**Figure 9.** Vertical profiles of the longitudinal, transversal and vertical advective transport of turbulent kinetic energy (by the time-averaged flow), in the longitudinal plane *y/d*=8.3. BA-R1 data set.

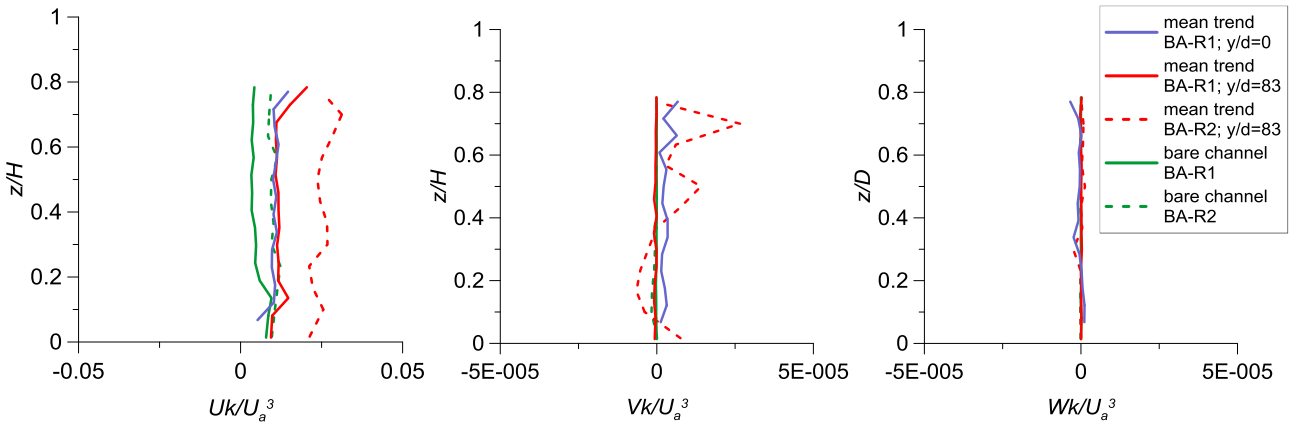



**Figure 10.** Mean trend of vertical profiles of the longitudinal, transversal and vertical advective transport of turbulent kinetic energy (by the time-averaged flow for all the assessed data

*4.2 Results of PA-F data set*

Figure 11a shows the horizontal distribution of the resultant horizontal velocity $Ut = \sqrt{U^2 + V^2}$ at *z/H*=0.42 along a stretch of the vegetated-bed (run PA-F). It can be seen in this figure the formation of alternating zones of high/low values of flow velocity. Figure 11b shows the vertical profiles of the averaged longitudinal *U* velocity, normalized by *Ua*, for different *x/d* positions: *x/d*=133.3 (i.e. at a distance of 40cm from the initial section *x*=0), *x/d*=266.6 (i.e. at a distance of 80cm from the initial section *x*=0), *x/d*=400.0 (i.e. at a distance of 120cm from the initial section *x*=0). The corresponding averaged profile (red line) is compared with the vertical profile (green line) obtained at position *x/d*=666.6 (i.e. at section distant 200 cm from the initial section) without vegetation on the bed. Unlike the case of absence of vegetation, in presence of vegetation the velocity profile shows the typical S-shape. In fact, the presence of dense vegetation generates a region of shear and a profile with an inflection point near the top of the canopy (see also Nepf, 2012a,b; Carollo et al., 2005; Termini, 2015; Termini, 2016a,b).

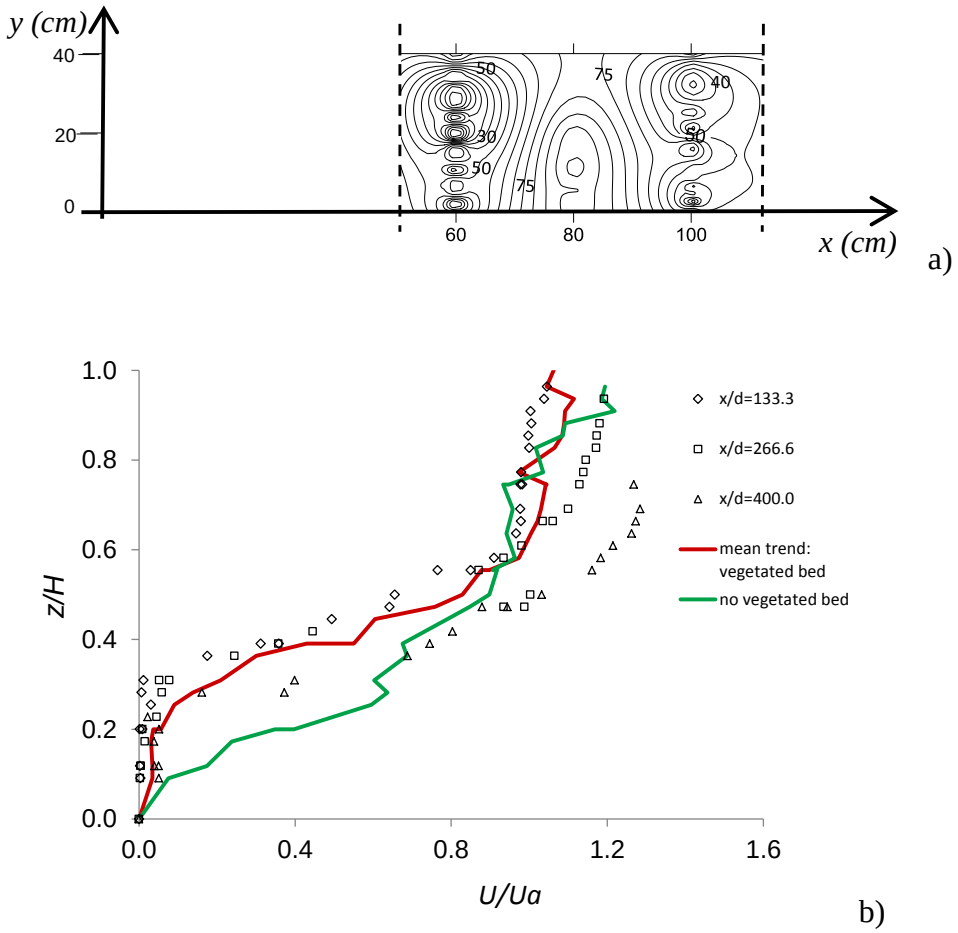



**Figure 11**. a) Horizontal map of the flow velocity [$U_t$ (cm/s)] distribution in the plane (*xy*) at *z/H*=0.42 along the vegetated-bed reach for PA-F data set; b) vertical profiles of *U/Ua* velocity component - PA-F data set.

Figure 12 shows the vertical profiles of the turbulent kinetic energy, normalized by the square of the mean flow velocity $U_a^2$, estimated at different locations along the channel axis. In this figure the profiles of the spatial average of turbulent kinetic energy and of the turbulent kinetic energy estimated at the position *x/d*=700.0 (i.e. at section distant 210cm from the initial section, without vegetation on the bed) both normalized by the square of the mean flow velocity $U_a^2$, are also reported.

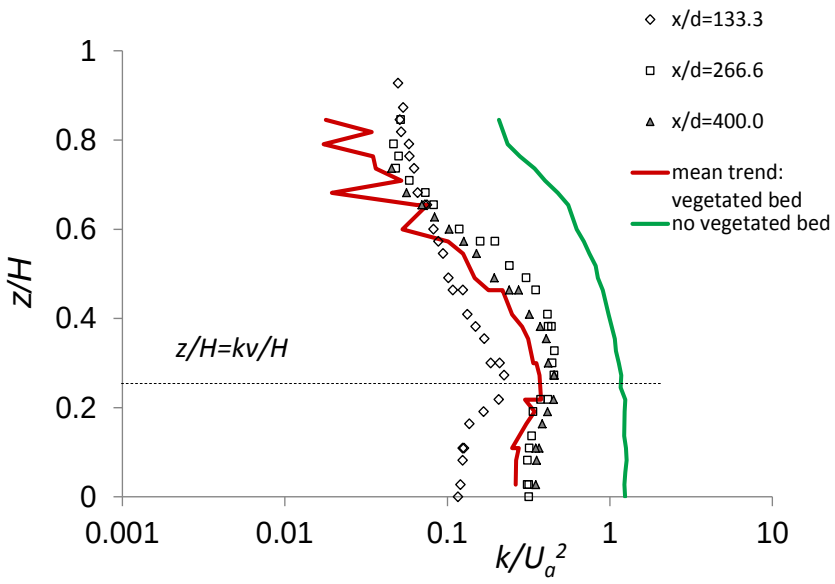



**Figure 12.** Vertical profiles of the normalized turbulent kinetic energy. PA-F data set.

This figure shows that in presence of vegetation the value of the turbulent kinetic energy increases inside the vegetated layer. It reaches a peak value approximately at a relative water depth equal to $z/H=k_v/H=0.24$. and it decreases towards the free surface. Thus, according to Nepf and Vivoni (2000), $k/U_a^2$ increases in the shear region. At the position *x/d*=700.0 (without vegetation on the bed) the turbulent kinetic energy shows a decreasing trend from the bed towards the free surface, as observed in the case of unobstructed flow for BA-R data set. In the absence of vegetation, $k/U_a^2$ assumes values greater than those obtained in the upstream positions with vegetation on the bed. This could be due to the fact that the presence of dense vegetation offers additional resistance determining flow velocity always less than that over no-vegetation condition (bare bed) (see also Nepf, 1999; 2012a,b).

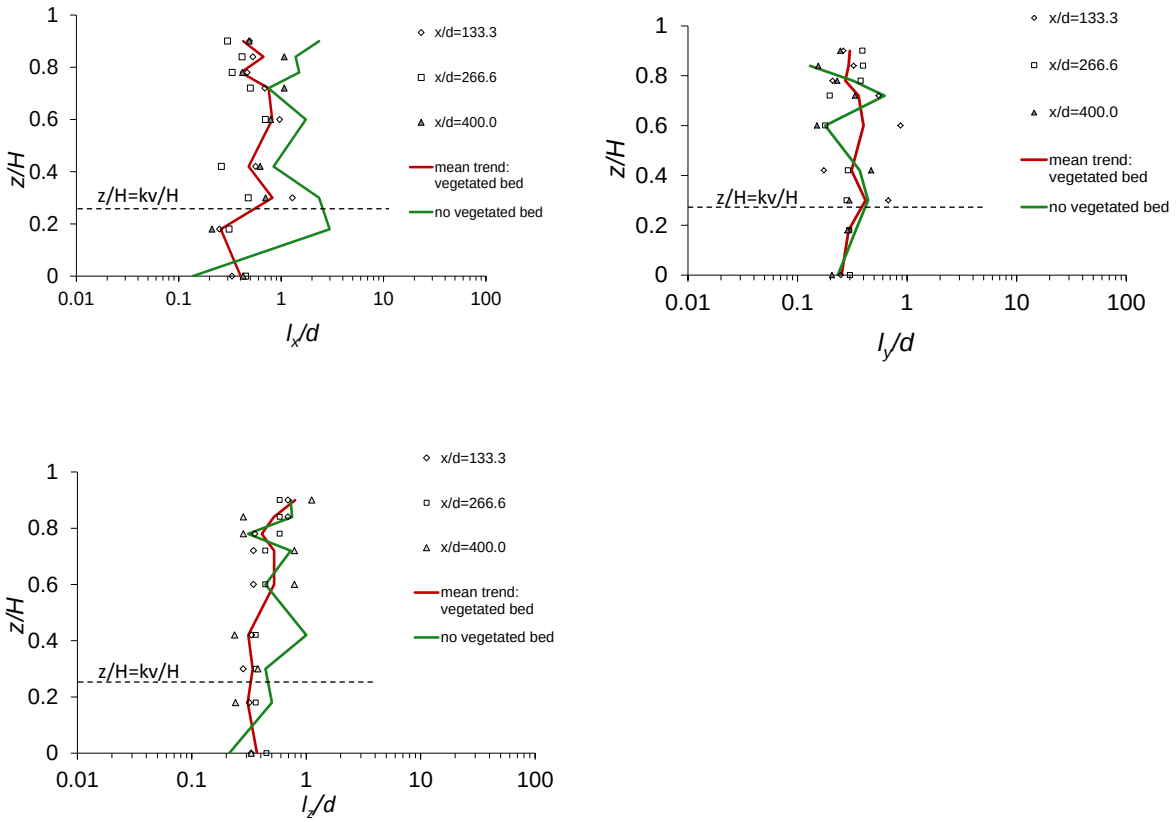



**Figure 13.** Vertical profiles of integral length scales *lx*, *ly* and *lz*, in the longitudinal plane *y*=0.20m. PA-F data set.

Figure 13 shows the integral turbulent lengths, normalized by *d*, along the directions *x*, *y*, *z*, estimated for the PA-F run. In this case, the order of magnitude of the integral scale *lx* remains quite invariant, i.e. O(d), even if a reduction is observed in the obstructed case. A similar behavior is also noted in the vertical and transversal directions, for the integral scales *ly* and *lz*. This is consistent with results obtained by Tanino and Nepf (2008) in random cylinder arrays with $\phi$=0.01÷0.35. It is noteworthy that in the case of the dense canopy the behavior for the turbulent length scales is nearly isotropic.

The vertical profiles of the dispersion coefficients *Kxx*, *Kyy* and *Kzz*, normalized by $U_a d$, are plotted in Figure 14. In this case, all the dispersion coefficients (*Kxx*, *Kyy*, *Kyy*) assume in presence of vegetation values lower than those obtained in absence of vegetation. This is particularly evident in the longitudinal direction.

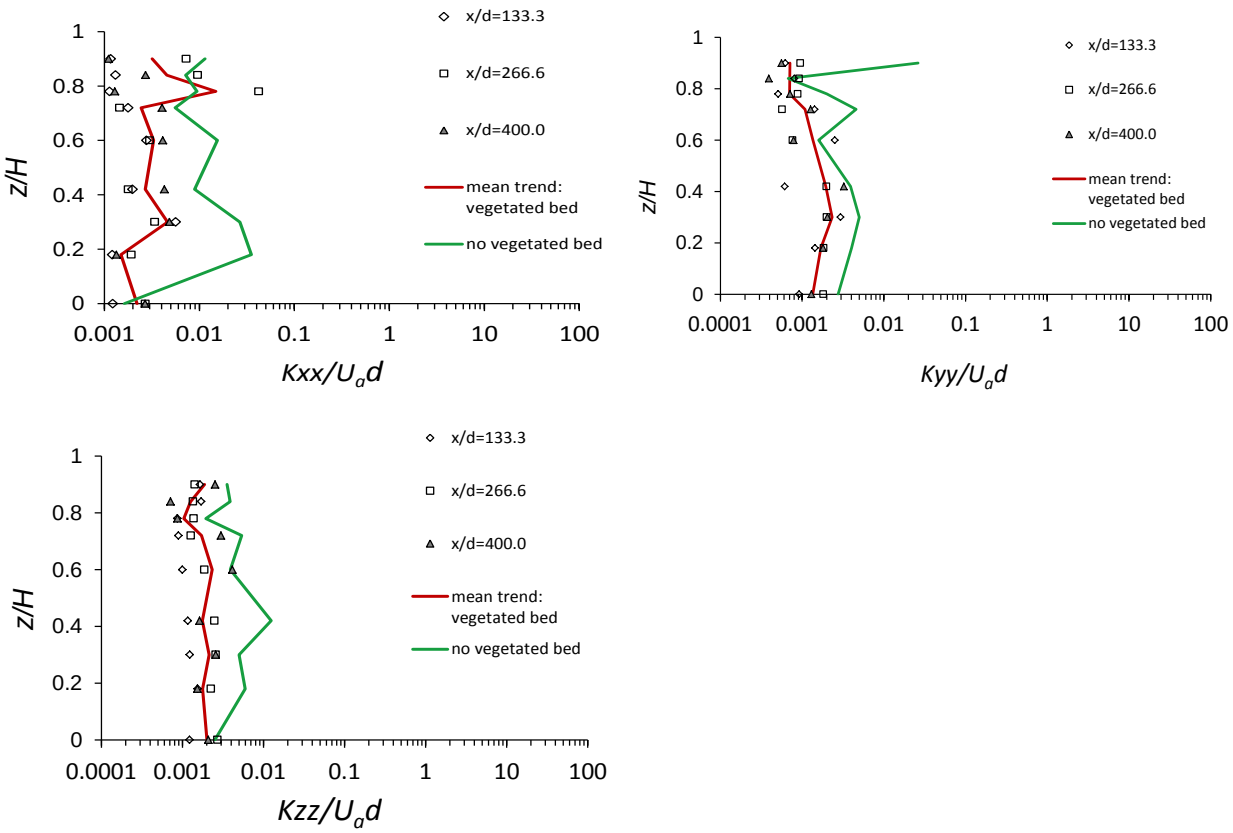



**Figure 14.** Vertical profiles of dispersion coefficients *Kxx*, *Kyy* and *Kzz*. PA-F data set.

The advective transport of $k$ by the time-averaged flow, normalized by $U_a^3$, is displayed in Figure 15. When vegetation is present, the spatially averaged transport in the transversal and vertical directions is around zero, while it assumes positive values in the unobstructed flow. In the longitudinal direction, the spatially averaged advective transport in presence of vegetation is reduced with respect to the unobstructed case. In both cases the spatially averaged advective transport shows an increasing trend from the bed towards the free surface, increasing in the shear region and reaching a maximum value at $z/H \cong 0.4$; then it decreases again.

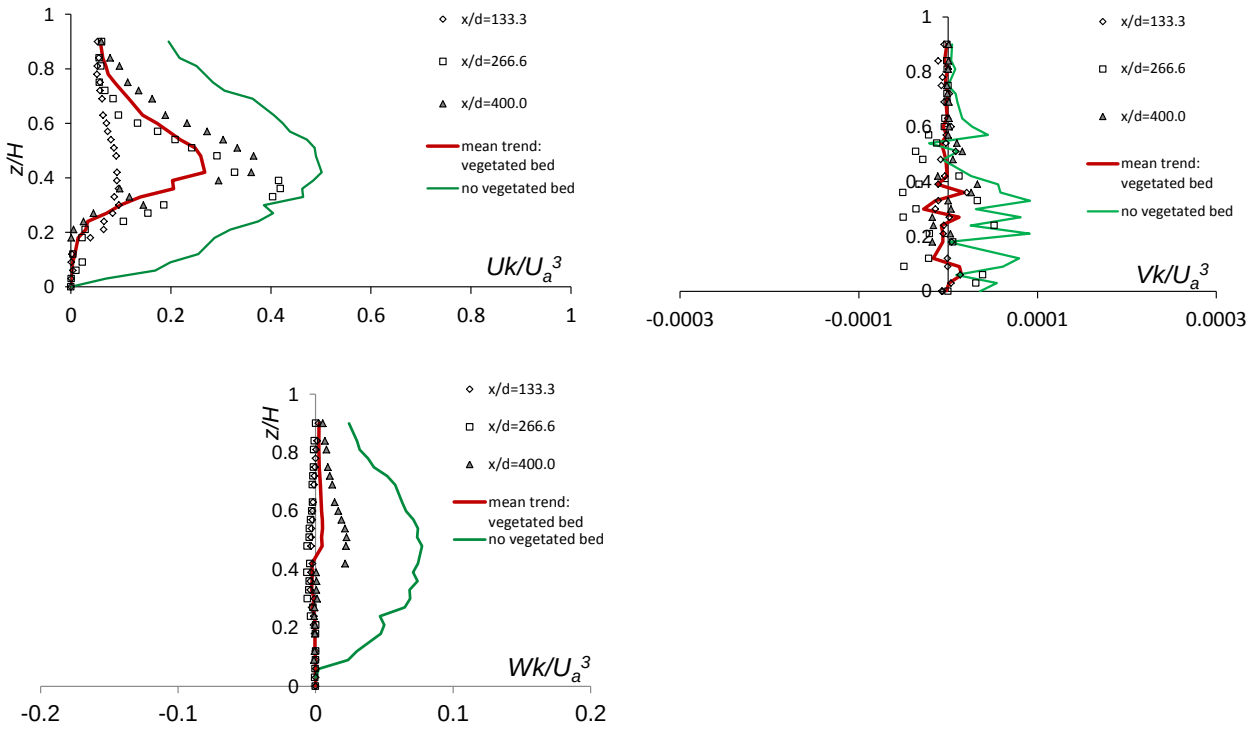



**Figure 15.** Vertical profiles of the longitudinal, transversal and vertical advective transport of turbulent kinetic energy (by the time-averaged flow). PA-F data set.

## 5. DISCUSSION

A reasonable analysis of the two examined data sets, which are characterized by very different canopies, rigid emergent and flexible submerged respectively, can be carried out only if we take in due count that: i) the value of *Ua* (thus of $Re_d$) characterizing the PA-F data set is about 5 times greater than the corresponding one of the BA-R data set, ii) the vegetation density *a* characterizing the PA-F data set is about 50 times greater than the corresponding one of the BA-R data set. As inferable from the following lines, the second of these two parameters strongly affects the experimental results.

Considering the distribution of the turbulent kinetic energy *k*, in the unobstructed case for both the data sets, a decreasing trend is noted from the bottom, where the turbulence is high because of the bed roughness, towards the surface, even if the vertical gradient of *k* is greater for the PA-F than for the BA-R observations. On the contrary, when the vegetation is present, the behavior in the two data sets is different. In fact, the low density of the rigid vegetation BA-R allows the flow to move inside the patch and the obstructive mechanism increases the turbulent kinetic energy compared to the not vegetated flow (Figure 4) as also noted in the experiments by Maji et al. (2016).

On the contrary, in the PA-F data set (Figure 12) the presence of the vegetation reduces the turbulent kinetic energy with respect to the not vegetated flow, because the densely distributed flexible stems act as a blockage, inducing an increased drag and a reduction of the mean flow U. This is consistent with results obtained by Nepf (1999; 2012a,b) by comparing flow velocity and kinetic energy profiles for different densities of canopy including the bare bed condition. It is also worth noting that in the BA-R experiments the observations are sensitive to the relative position of the measuring point with respect to the stems.

The analysis of the integral length scales leads to the following deductions. As already written, the unobstructed flow of the BA-R case shows values of *lx* of order of O(*H*), while in the obstructed flow *lx* assumes order O(*d*) or O(*s*) depending on the position relatively to the stems (Figure 6). Namely, in the wake region it is O(*d*) while between stems it is O(*s*). This is a novel result with respect to previous studies (Nepf, 1997; 1999; Shivpure et al., 2016). Even the reduction of *lz* is noted for the vegetated case. While *lx* and *lz* values reduce, values of the transversal *ly* increase, thus expecting turbulent eddies flattened in the longitudinal and vertical direction but transversally stretched, with respect to the unobstructed flow. This behavior reveals the anisotropy of turbulence spreading in the case of sparse vegetation. In the PA-F experiment the *lx*, *ly* and *lz* are always reduced when facing the flexible stems, with order of magnitudes comparable to *d* (Figure 13). Therefore, in the dense canopy, turbulence is characterized by isotropy. This result furtherly proves that the dense vegetation intercepts and blocks the turbulent eddies, independently on the direction, especially due to the overlapping of stem wakes. On the contrary, the rigid and sparse vegetation allows a transversal spreading of turbulent patterns, thus making the transversal direction a favorite path for turbulent eddies.

The dispersion coefficients of the BA-R data set show vertical trends analogous to those of the integral length scales, confirming a reduction of the possible dispersion of tracers in the longitudinal direction and an increase along the transversal one (Figures 7 and 8). Further, considering eq. (12) used for the computation of *Kij* coefficients, it should be noted that in the vegetated case the reduction of *lx* prevails on the increase of $\sqrt{k}$, thus providing reduced *Kxx* values. Again, this dispersion mechanism is consistent with the sparse location and the pattern of the rigid canopy, frontally impeding the development of the turbulent eddies, but allowing their development transversally on both sides. Therefore, the anisotropy of turbulence is furtherly proved, as well as the presence of secondary currents, which advect turbulence spanwisely, confirming also results by Nezu and Onitsuka (2001).

The longitudinal advective transport of *k* in the BA-R experiment was expected lower in the vegetated flow than in the unobstructed one. On the contrary, it resulted greater for the vegetated

case (Figures 9 and 10). This could be explained considering that in the vegetated flow, two competing effects are present, i.e. reduced velocity and increased turbulence (Nepf, 2012a,b). These opposing tendencies are responsible for an initial increasing of turbulence due to the presence of sparse stems, as in the BA-R case (Figure 4), but eventually turbulence decreases when the vegetation density increases further, as in the PA-F case (Figure 12). In fact, the behavior within the flexible stems of the PA-data set shows turbulent eddies smaller in size (Figure 13), with a consequent reduction of the dispersion coefficients along all the three directions (Figure 14). The flexible and dense system behaves as a 'filter' which determines a reduction of the turbulent flow features and prevents high rates of the advective transport of *k* (Figure 15). This is consistent with previous literature results (Pietri et al., 2009; Nepf, 2012a,b) demonstrating that, at stem scale, the length scale of the developing vortices is set by the stem diameter, and this length scale partially controls the characteristic eddy size which develop within and between the vegetated elements (Termini, 2016b; 2017).

Therefore, consistently with eq. (4) and eq. (9), applying the analogy between the transport of TKE and the transport of a solute/tracer, it can be highlighted that the transport of a scalar in a canopy is heterogeneous and spatially variable and is strictly governed by the density of the canopy. The consequence is that only for high values of vegetation density, the transport and dispersion of a tracer is strongly inhibited along all the three directions. In the case of sparse vegetation, a transversal path is allowed to turbulent eddies and consequently also to tracer transport, while the advective longitudinal transport depends on the relative prevalence of channel velocity or turbulence. It could be argued that even suspended sediments could experience an analogous mechanism of spreading.

## 6. CONCLUDING REMARKS

Experiments with vegetated channels were executed in the case of both flexible submerged and rigid emergent canopies. Specifically, the process transport and dispersion of tracers was investigated, once noted that it resembles the transport and dispersion of turbulent kinetic energy *k*.

In presence of vegetation, for both canopy configurations a reduction of the mean longitudinal velocity is experienced. On the contrary, the behavior of *k* is opposite. In fact, with respect to the not vegetated flow, the sparse and rigid vegetation BA-R induces an increasing of *k*, while in the PA-F data set the dense and flexible stems reduce the turbulent kinetic energy, acting as a filter.

Referring to the integral length scales, in the sparse canopy (BA-R) the longitudinal turbulent scale $l_x$ of the unobstructed channel is of O($H$), while it is reduced by the presence of the stems and scaled by $d$ or $s$, according to the position relatively to the stems. Namely, in the wake region it is

O(*d*) while between stems it is O(*s*). This heterogenous behavior, locally variable and dependent on the position, is a novel aspect with reference to previous researches. The vertical length scale lz is reduced while the transversal length scale *ly* is increased by the presence of the stems, thus expecting turbulent eddies flattened in the longitudinal and vertical direction but transversally stretched, with respect to the unobstructed flow. This behavior reveals the anisotropy of turbulence spreading in the case of sparse vegetation.

In the dense canopy (PA-F) the *lx*, *ly* and *lz* turbulent scales are always reduced in presence of vegetation, with order of magnitudes even smaller than *d*. As an interesting result, in the dense canopy, turbulence is characterized by isotropy.

The trends for the dispersion coefficients follow those of the turbulent scales. In fact, in presence of vegetation, they are reduced along the three directions in the PA-F data set, while in the BA-R data set a reduction is noted only for the longitudinal and vertical ones.

The analysis of the experimental results highlight that again the density of the canopy is the key parameter in the advective processes. In fact, the transport of *k* and therefore of a possible solute is strictly dependent on the density of the canopy. Only for high values of vegetation density, the transport and dispersion of a tracer is obstructed along all directions. In the case of sparse vegetation, a favorite transversal path is allowed to turbulent eddies and consequently also to tracers transport. In the longitudinal direction, the advective transport depends on the relative prevalence of channel velocity or turbulence.

**REFERENCES**

Ben Meftah M., Mossa M. Prediction of channel flow characteristics through square arrays of emergent cylinders. Phys. Fluids, 2013; 25(4): 1–21.

Ben Meftah M., De Serio F., Mossa M.. Hydrodynamic behavior in the outer shear layer of partly obstructed open channels. Phys. Fluids, 2014; 26(6): 1–19.

Ben Meftah M, De Serio F, Malcangio D, Mossa M, Petrillo AF. Experimental study of a vertical jet in a vegetated crossflow. Journal of Environmental Management, 2015; 9.

Ben Meftah M., Mossa M. Partially obstructed channel: Contraction ratio effect on the flow hydrodynamic structure and prediction of the transversal mean velocity profile. Journal of Hydrology, 2016; 542.

Camporeale,C., Perona P., Porporato A., Ridolfi L. On the long-term behavior of meandering rivers. Water Resour. Res., 2005; 41: W12403.

Carollo FG., Ferro V., Termini D. Flow Resistance Law in Channels with Flexible Submerged Vegetation, J. of Hydr. Eng. 2005; 131: 554-564.

Costanza R., D'Arge R., De Groot R., Farber S., Grasso M., Hannon B., Limburg K., Naeem S., Oneill RV., Paruel, J., Raskin RG., Sutton P., van den Belt M. The value of the world's ecosystem services and natural capital. Nature, 1997; 387: 253-260.

Crosato A, Saleh MS. Numerical study on the effects of floodplain vegetation on river planform style. Earth Surf. Process. Landforms, 2011; 36: 711–720.

Finnigan, J.J. Turbulent transport in flexible plant canopies. In the Forest-Atmosphere Interaction (ed. B.A. Hutchison and B.B. Hicks) 1985; 443-480.

Ghisalberti M., Nepf H. The limited growth of vegetated shear layers. Water. Resour. Res., 2004; 40: W07502.

Ghisalberti M., Nepf H. Mass transfer in vegetated shear flows. Environ Fluid Mech, 2005; 5(6): 527-551.

Ghisalberti M., Nepf H. The structure of the shear layer over rigid and flexible canopies. Environ Fluid Mech., 2006; 6(3):277-301.

Ghisalberti M., Nepf H. Shallow flows over a permeable medium: the hydrodynamics of submerged aquatic canopies. Transport in Porous Media, 2009; 78(2): 309–326.

Gregory SV., Swanson FJ., McKee WA., Cummins KW. An ecosystem perspective of riparian areas. BioScience, 1991; 41: 540–551.

Gurnell A. Plants as river system engineers, Earth Surf. Processes Landforms, 2014; 39(1): 4-25.

Ikeda S., Kanazawa M. Three-Dimensional organized vortices above flexible water plants. Journal of Hydraulic Engineering, 1996; 122(11).

Kemp JL., Harper DM., Crosa GA. The habitat-scale eco-hydraulics of rivers. Ecol. Eng., 2000; 16(1): 17–29.

Lima AC., Izumi, N. Linear stability analysis of open-channel shear flow generated by vegetation. J. Hydraul. Eng., 2014; 140: 231–240.

Liu C., Nepf H. Sediment deposition within and around a finite patch of model vegetation over a range of channel velocity, Water Resour. Res., 2016; 52: 600–612.

López F, García M..Open-channel flow through simulated vegetation: suspended sediment transport modeling. Water Resources Research 1998; 34: 2341–2352.

Lotsari E., Thorndycraft V., Alho P., Prospects and challenges of simulating river channel response to future climate change. Progress in Physical Geography, 2015; 1–31.

Maji S., Pal D., Hanmaiahgari PR., Pu JH. Phenomenological Features of Turbulent Hydrodynamics in Sparsely Vegetated Open Channel Flow. Journal of Applied Fluid Mechanics 2016; 9(6): 2865-2875.

Marion A., Zaramella M., Bottacin-Busolin A. Solute transport in rivers with multiple storage zones: The STIR model. Water Resources Research, 2008; 44:W10406.

Marois DE., Mitsch WJ., Song K., Miao S., Zhang L., Nguyenet CT. Estimating the Importance of Aquatic Primary Productivity for Phosphorus Retention in Florida Everglades Mesocosms. Wetlands, 2015; 35(2): 357-368.

Mossa M., De Serio F., Rethinking the process of detrainment: jets in obstructed natural flows. Scientific Report, 2106; 6: 39103.

Naden P., Rameshwaran P., Mountford O., Robertson C. The influence of macrophyte growth, typical of eutrophic conditions, on river flow velocities and turbulence production. Hydrol. Processes, 2006; 20(18): 3915–3938,

Nepf H., Mugnier C., Zavistoski R. The effects of vegetation on longitudinal dispersion. Estuarine, Coastal and Shelf Science, 1997; 44: 675-684.

Nepf, H. Drag, turbulence and diffusivity in flow through emergent vegetation. Water Res. Res., 1999; 35(2): 479-489.

Nepf H., Ghisalberti M., White B., Murphy E. Retention time and dispersion associated with submerged aquatic canopies. Water Resource Res., 2007; 43: W04422.

Nepf, H. Flow and transport in regions with aquatic vegetation, Annu. Rev. Fluid Mech., 2012a; 44: 123–142.

Nepf, H. Hydrodynamics of vegetated channels, J. Hydraul. Res. 2012b; 50(3): 262–279.

Nepf H., Vivoni E. Flow structure in depth-limited, vegetated flow. Journal of Geophysical Research, 2000; 105(C12): 28547-28557.

Nezu I., Onitsuka K. Turbulent structures in partly vegetated open-channel flows with LDA and PIV measurements. J. Hydr. Res. 2001; 39(6): 629–642.

Okubo A., Oceanic diffusion diagrams. Deep Sea Res. 1971; 18: 789-802.

Oldham CE., Sturman JJ. The effect of emergent vegetation on convective flushing in shallow wetlands: Scaling and experiments. Limnol. Oceanogr.,2001; 46(6): 1486–1493.

Perucca E., Camporeale C., Ridolfi L. Estimation of the dispersion coefficient in rivers with riparian vegetation. Advances in Water Resources, 2009; 32: 78-87.

Pietri L., Petroff A., Amielh M. Anselmet F. Turbulence characteristics within sparse and dense canopies. Environ Fluid Mech 2009; 9: 297.

Poggi D., Porporato A., Ridolfi L., Albertson JD., Katul GG., The effect of vegetation density on canopy sub-layer turbulence, Boundary Layer Meteorol., 204; 111: 565–587.

Poggi D., Krug C., Katul GG. Hydraulic resistance of submerged rigid vegetation derived from first-order closure models. Water Resour. Res., 2009; 45: W10442.

Pollen N., Simon A. Estimating the mechanical effects of riparian vegetation on stream bank stability using a fiber bundle model. Water Resource Research, 2005; 41: W07025.

Raupach MR, Thom AS. Turbulence in and above plantcanopies. Annu Rev Fluid Mech 1981; 13: 97–129.

Raupach M., Shaw R. Averaging procedures for flow within vegetation canopies. Boundary Layer Meteorol. 1982; 22: 79-90.

Ricardo AM., Di Carlo S., Sanches P., Franca MJ., Schleiss AJ., Ferreira RML. Vortex interaction in patches of randomly placed emergent cylinders. In River Flow 2014, Schleiss et al. (eds), Lausanne, Switzerland, 2014; 63-69.

Righetti M, Armanini A. Flow resistance in open channel flow with sparsely distributed bushes. Journal of Hydrology 2002; 269: 55 -64.

Righetti M. Flow analysis in a channel with flexible vegetation using double-averaging method. Acta Geophysica 2008; 56(3): 801–823.

Rodi W. Turbulence model and their application in Hydraulics – a state of the art review, IAHR Monograph 1984, Balkema, Rotterdam.

Rubol S., Battiato I., de Barros FPJ. Vertical dispersion in vegetated shear flows. Water Resour. Res., 2016; 52: 8066–8080.

Sandercock PJ., Hooke JM. Vegetation effects on sediment connectivity and processes in an ephemeral channel in SE Spain. Journal of Arid Environments 2011; 75: 239-254.

Schultz RC., Colletti JP. Isenhart TM., Simpkins WW., Mize CW., Thompson ML. Design and placement of a multi-species riparian buffer system. Agroforest. Syst., 1995; 29: 201-226.

Shivpure V., Bebina Devi T., Kumar B. Turbulent characteristics of densely flexible submerged vegetated channel, Journal of Hydraulic Engineering 2016; 22(2): 220-226,

Shucksmith JD., Boxall JB., Guymer I. Effects of emergent and submerged natural vegetation on longitudinal mixing in open channel flow. Water Resources Research, 2010; 46: W04504.

Shucksmith JD., Boxall JB., Guymer I. Determining longitudinal dispersion coefficients for submerged vegetated flow. Water Resources Research, 2011; 47: W10516.

Tanino Y., Nepf H. Lateral dispersion in random cylinder arrays at high Reynods number. Journal of Fluid Mechanics, 2008; 600: 339-371.

Taylor GI. Statistical Theory of Turbulence. Proceedings of the Royal Society of London. Series A, Mathematical and Physical Sciences 1935; 151(873): 421-444

Termini D. Effect of vegetation on fluvial erosion processes: experimental analysis in a laboratory flume. Procedia Environmental Sciences 2013; 19: 904 – 911.

Termini D. Flexible vegetation behaviour and effects on flow conveyance: experimental observations. International Journal of River Basin Management 2015; 401-411.

Termini D. Reduction of scouring downstream of a rigid bed by means of a vegetated carpet: experimental investigation in a laboratory flume. Environmental Fluid Mechanics, 2016a; 1111-1127.

Termini D. Experimental analysis of the effect of vegetation on flow and bed shear stress distribution in high-curvature bends. Geomorphology, 2016b

Termini D., Sammartano V. Morphodynamic processes downstream of man-made structural interventions: experimental investigation of the role of turbulent flow structures in the prediction of scour downstream of a rigid bed. Physics and Chemistry of the Earth, 2012; 49: 18–31.

Termini D. Vegetation effects on cross-sectional flow in a large amplitude meandering bend. Journal of Hydraulic Research, 2017, 55(3).

Ting FCK., Kirby JT. Observation of undertow and turbulence in a laboratory surf zone. Coastal Engineering, 1994; 24: 51– 80.

Ting FCK., Kirby JT. Dynamics of surf-zone turbulence in a strong plunging breaker. Coastal Engineering, 1995; 24: 177–204.

Ting FCK., Kirby JT. Dynamics of surf-zone turbulence in a spilling breaker. Coastal Engineering, 1996; 27: 305–310.

White B., Nepf H. Shear instability and coherent structures in shallow flow adjacent to a porous layer. Journal of Fluid Mechanics, 2007a; 593:1-32.

White B., Nepf H.  A vortex-based model of velocity and shear stress in a partially vegetated shallow channel. Water Res. Res., 2007b; 44(1): W01412.

Zong L., Nepf H. Vortex development behind a finite porous obstruction in a channel, J. Fluid Mech., 2012; 691: 368–391.